

Let the Data Choose its Features: Differentiable Unsupervised Feature Selection

Ofir Lindenbaum^{1*} Uri Shaham^{1*} Jonathan Svirsky²
Erez Peterfreund³
Yuval Kluger^{1†}

¹Yale University, USA; ² Technion, Israel; ³ Hebrew University, Israel

[†]Corresponding author. E-mail: yuval.kluger@yale.edu

Address: 333 Cedar St, New Haven, CT 06510, USA

* These authors contributed equally.

Abstract

Scientific observations often consist of a large number of variables (features). Identifying a subset of meaningful features is often ignored in unsupervised learning, despite its potential for unraveling clear patterns hidden in the ambient space. In this paper, we present a method for unsupervised feature selection, tailored for the task of clustering. We propose a differentiable loss function which combines the graph Laplacian with a gating mechanism based on continuous approximation of Bernoulli random variables. The Laplacian is used to define a scoring term that favors low-frequency features, while the parameters of the Bernoulli variables are trained to enable selection of the most informative features. We mathematically motivate the proposed approach, and demonstrate that in the high noise regime, it is crucial to compute the Laplacian on the gated inputs, rather than on the full feature set. Experimental demonstration of the efficacy of the proposed approach and its advantage over current baselines is provided using several real-world examples.

1 Introduction

Recently there has been a growing interest in the machine learning community towards unsupervised and self-supervised learning. This was motivated by impressive empirical results demonstrating the benefits of analyzing large amounts of unlabeled data (for example in natural language processing). In many scientific domains, such as biology and physics, the growth of computational and storage resources, as well as technological advances for measuring numerous features simultaneously, makes the analysis of large, high dimensional datasets an important research need. In such datasets, discarding irrelevant (i.e. noisy and information-poor) features may reveal clear underlying natural structures that are otherwise hidden in the high dimensional space. We refer to these uninformative features as “nuisance features”. While nuisance features are mildly harmful in the supervised regime, in the unsupervised regime discarding such features is crucial and may determine the success of downstream analysis tasks (e.g., clustering or manifold learning). Some of the pitfalls caused by nuisance features could be mitigated using an appropriate unsupervised feature selection method.

The problem of feature selection has been studied extensively in machine learning and statistics. Most of the research is focused on supervised feature selection, where identifying a subset of informative features has benefits such as reduction in memory and computations, and improved generalization performance and interpretability. Filter methods, such as [1, 2, 3, 4, 5, 6] attempt to remove irrelevant features prior to learning a model. Wrapper methods [7, 8, 9, 10, 11] use the outcome of a model to determine the relevance of each feature. Embedded methods, such as [12, 13, 14, 15, 16] aim to learn the model while simultaneously select the subset of relevant features.

Unsupervised feature selection methods mostly focus on two main tasks: clustering and dimensionality reduction or manifold learning. Among studies which tackle the former task, [17, 18, 19] use autoencoders to identify features that are sufficient for reconstructing the data. Other clustering-dedicated unsupervised feature selection methods assess the relevance of each feature based on different statistical or geometric measures. Entropy, divergence and mutual information are used in [20, 21, 22, 23, 24] to identify features which are informative for clustering the data. A popular tool for evaluating features is the graph Laplacian [25, 26]. The Laplacian Score (LS) [27], evaluates the importance of each feature by its ability to preserve local structure. The features which most preserve the manifold structure (captured by the Laplacian) are retained. Several studies, such as [28, 29, 30], extend the LS based on different spectral properties of the Laplacian.

While these methods are widely used in the feature selection community, they rely on the success of the Laplacian in capturing the “true” structure of the data. We argue that when the Laplacian is computed based on all features, it often fails to identify the informative ones. This may happen in the presence of a large number of nuisance features, when the variability of the nuisance features masks the variability associated with the informative features. Scenarios like this are prevalent in areas such as bioinformatics, where a large number of biomarkers are measured to characterize developmental and chronological biology processes such as cell differentiation or cell cycle. These processes may depend merely on a few biomarkers. In these situations, it is desirable to have an unsupervised method that can filter nuisance features prior to the computation of the Laplacian.

In this study, we propose a differentiable objective for unsupervised feature selection. Our proposed method utilizes trainable stochastic input gates, trained to select features with high correlation with the leading eigenvectors of a graph Laplacian that is computed based on these features. This gating mechanism allows us to re-evaluate the Laplacian for different subsets of features and thus unmask informative structures buried by the nuisance features. We will demonstrate, both experimentally and analytically, that the proposed approach outperforms several current unsupervised feature selection baselines.

2 Preliminaries

Consider a data matrix $\mathbf{X} \in \mathbb{R}^{n \times d}$, with d dimensional observations $\mathbf{x}_1, \dots, \mathbf{x}_n$. We refer to the columns of \mathbf{X} as features $\mathbf{f}_1, \dots, \mathbf{f}_d$, where $\mathbf{f}_i \in \mathbb{R}^n$ and we assume that features are centered and normalized such that $\mathbf{1}^T \mathbf{f}_i = 0$ and $\|\mathbf{f}_i\|_2^2 = 1$. We assume that the data has an inherent structure, determined by a small subset of the features \mathcal{S}^* and that other features are nuisance variables. Our goal is to identify the subset of relevant features \mathcal{S}^* and discard the remaining ones.

2.1 Graph Laplacians

Given n data points, a kernel matrix is a $n \times n$ matrix \mathbf{K} so that $\mathbf{K}_{i,j}$ represents the similarity between \mathbf{x}_i and \mathbf{x}_j . A popular choice to construct such matrix is using a Gaussian kernel

$$\mathbf{K}_{i,j} = \exp\left(-\frac{\|\mathbf{x}_i - \mathbf{x}_j\|^2}{2\sigma_b^2}\right),$$

where σ_b is a user-defined bandwidth (chosen, for example, based on the median of the 1-nearest neighbors of all points). The unnormalized graph Laplacian matrix is defined as $\mathbf{L}_{\text{un}} = \mathbf{D} - \mathbf{K}$, where \mathbf{D} is a diagonal matrix \mathbf{D} , whose elements $\mathbf{D}_{i,i} = \sum_{j=1}^n \mathbf{K}_{i,j}$ correspond to the degrees of the points $i = 1, \dots, n$. The random walk graph Laplacian is defined as $\mathbf{L}_{\text{rw}} = \mathbf{D}^{-1}\mathbf{K}$, and expresses the transition probabilities of a random walk to move between data points. Graph Laplacian matrices are extremely useful in many unsupervised machine learning tasks. In particular, it is known that the eigenvectors corresponding to the small eigenvalues of the unnormalized Laplacian (or the large eigenvalues of the random walk Laplacian) are useful for embedding the data in low dimension (see, for example, [31]).

2.2 Laplacian Score

Following the success of Laplacian Eigenmaps [26] and Spectral Clustering [25], the authors in [27] have presented an unsupervised measure for feature selection, termed Laplacian Score (LS). The LS evaluates each feature based on its correlation with the leading eigenvectors of the graph Laplacian.

At the core of the LS method, the score of feature \mathbf{f} is determined by the quadratic form $\mathbf{f}^T \mathbf{L} \mathbf{f}$, where $\mathbf{L} = \mathbf{L}_{\text{un}}$ is the unnormalized graph Laplacian. Since

$$\mathbf{f}^T \mathbf{L} \mathbf{f} = \sum_{i=1}^n \lambda_i \langle \mathbf{u}_i, \mathbf{f} \rangle^2,$$

where $\mathbf{L} = \sum_{i=1}^n \lambda_i \mathbf{u}_i \mathbf{u}_i^T$ is the eigen-decomposition of \mathbf{L} , the score is smaller when \mathbf{f} has a larger component in the subspace of the smallest eigenvectors of \mathbf{L} . Such features can be thought of as “informative”, as they respect the graph structure. Eigenvalues of the Laplacian can be interpreted as frequencies, and eigenvectors corresponding to larger eigenvalues of \mathbf{L}_{un} (or smaller eigenvalues of \mathbf{L}_{rw}) oscillate faster. Based on the assumption that the interesting underlying structure of the data (e.g. clusters) depends on the slowly varying features in the data, [27] proposed to select the features with the smallest scores.

2.3 Stochastic Gates

Due to the enormous success of gradient decent-based methods, most notably in deep learning, it is appealing to try to incorporate discrete random variables into a differentiable loss functions designed to retain the slow varying features in the data. However, the gradient estimates of discrete random variables tend to suffer from high variance [32]. Therefore, several authors have proposed continuous approximations of discrete random variables [33, 34]. Such relaxations have been used for several applications, such as model compression [35], discrete softmax activations [36] and feature selection [13]. Here, we use a Gaussian-based relaxation of Bernoulli variables, termed Stochastic Gates (STG) [13] which is differentiated based on the reparameterization trick [37, 38].

We denote the STG vector by $\tilde{\mathbf{Z}} \in [0, 1]^d$, parametrized by $\mu \in \mathbb{R}^d$, where each entry is defined as

$$\tilde{Z}_i = \max(0, \min(1, \mu_i + \epsilon_i)), \quad (1)$$

where μ_i is a learnable parameter, ϵ_i is drawn from $\mathcal{N}(0, \sigma^2)$ and σ is fixed throughout training. This approximation can be viewed as a clipped, mean-shifted, Gaussian random variable. In Fig. 1 we illustrate the gating mechanism; examples of the densities of \tilde{Z}_i for different values of μ_i are shown in Fig. 2.

Multiplication of each feature by its corresponding gate enables us to derive a fully differentiable feature selection method. At initialization $\mu_i = 0.5, i = 1, \dots, d$, so that all gates approximate a "fair" Bernoulli variable. The parameters μ_i can be learned via gradient decent optimization by incorporating the gates in a differentiable loss term. To encourage feature selection in the supervised setting, [13] proposed a differentiable regularization term defined by

$$r(\tilde{\mathbf{Z}}) = \sum_{i=1}^d \mathbb{P}(\tilde{Z}_i \geq 0) = \sum_{i=1}^d \left(\frac{1}{2} - \frac{1}{2} \operatorname{erf} \left(-\frac{\mu_i}{\sqrt{2}\sigma} \right) \right), \quad (2)$$

where $\operatorname{erf}()$ is the Gauss error function. The term (2) penalizes open gates, so that gates corresponding to features that are not useful for predicting the supervised objective function are encouraged to transition into a closed state (which is the case for small μ_i).

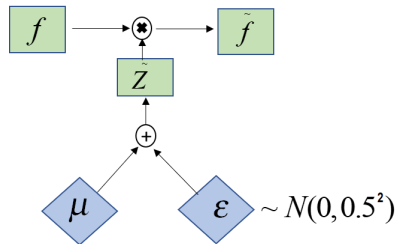


Figure 1: The stochastic gate \tilde{Z} is defined via the reparameterization trick [37, 38]. Standard Gaussian noise is injected and shifted by a trainable parameter μ_i , the result is thresholded to

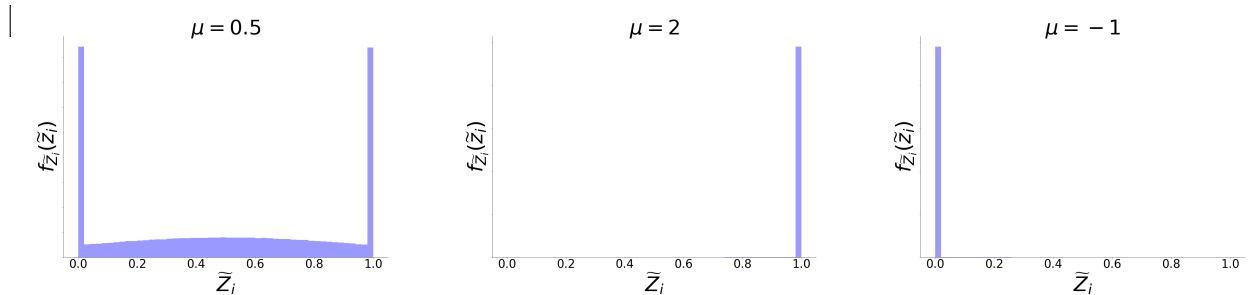


Figure 2: Three examples of the density of the stochastic gate \tilde{Z}_i . Left: at initialization $\mu_i = 0.5$ and the gate approximates a 'fair' Bernoulli variable. Middle: the distribution at $\mu_i = 2$ approximates a deterministic open gate. Right: the distribution at $\mu_i = -1$ approximates a 'closed' gate.

3 Demonstration of the Importance of Unsupervised Feature Selection in High Dimensional Data with Relevant and Irrelevant Nuisance Features

We first demonstrate the importance of feature selection in unsupervised learning when the data contains nuisance variables, by taking a diffusion perspective. Then, we use a simple two cluster

model to analyze how Gaussian nuisance dimensions affect clustering capabilities.

3.1 A Diffusion Perspective

Consider the following 2-dimensional dataset, known as “two-moons”, shown in the top-left panel of Fig. 3. We augment the data with k “nuisance” dimensions, where each such dimension is composed of i.i.d $\text{unif}(0, 1)$ entries. As one may expect, when the number of nuisance dimensions is large, the amount of noise (manifested by the nuisance dimensions) dominates the amount of signal (manifested by the two “true” dimensions). Consequently, attempts to recover the true structure of the data (say, using manifold learning or clustering) are likely to fail.

We will now analyze the above scenario from a diffusion perspective. Data is considered to be clusterable when the time it takes a random walk starting in one cluster to transition to a point outside the cluster is long. The exit times from different clusters are manifested by the leading eigenvalues of the Laplacian matrix $\mathbf{L}_{\text{rw}} = \mathbf{D}^{-1}\mathbf{K}$, for which the large eigenvalues (and their corresponding eigenvectors) are the ones that capture different aspects of the main data structures (see, for example, [39]). Each added nuisance dimension increases the distance between a point and its “true” nearest neighbors along one of the “moon” manifolds. In addition, the noise creates spurious similarities between points, regardless of the cluster they belong to. Overall, this shortens the cluster exit times. This phenomenon can be captured by the second largest eigenvalue λ_2 of \mathbf{L}_{rw} (the largest eigenvalue $\lambda_1 = 1$ carries no information as it corresponds to the constant eigenvector $\boldsymbol{\psi}_1$), which decreases as the number of nuisance dimensions grows, as is shown in the top right panel of Fig. 3. The fact that λ_2 decreases implies that the diffusion distances [39] in the graph decrease as well, which in turn means that the graph becomes more connected, and hence less clusterable. A similar view may be obtained by observing that the second smallest eigenvalue of the un-normalized graph Laplacian $\mathbf{L}_{\text{un}} = \mathbf{D} - \mathbf{W}$, also known as Fiedler number or algebraic connectivity, grows with the number of nuisance variables. The fact that the graph becomes less clusterable as more nuisance dimensions are added is also manifested by the eigenvector $\boldsymbol{\psi}_2$ corresponding to the second largest eigenvalue of \mathbf{L}_{rw} (or the second smallest eigenvalue of \mathbf{L}_{un}), which becomes less representative of the original cluster structure (bottom left panel of Fig. 3).

Altogether, this means that in order for the data to be clusterable, the noisy features ought to be removed. One may argue that principal component analysis can be used to retain the signal features while removing the noise. Unfortunately, as shown in the bottom right panel of Fig. 3, projecting the data onto the first two principal directions does not yield the desired result, as the variance along the noise directions is larger than along the signal ones. In the next sections we will describe our differentiable unsupervised feature selection approach, and demonstrate that it does succeed to recognize the important patterns of the data in this case.

3.2 Analysis of Clustering with Gaussian Nuisance Dimensions

In order to mathematically observe the effect of nuisance dimensions, in this section we consider a simple example where all noise arises from such dimensions. Specifically, consider data of $2n$ points in \mathbb{R} , where of n which are at $0 \in \mathbb{R}$ and the remaining ones are at $r > 0$, i.e., each cluster is concentrated at a point. Next, we add d nuisance dimensions, so that for each point $1, \dots, n$ and each nuisance dimension we sample a iid $N(0, 0.5^2)$ value. Altogether the data with nuisance dimensions now lies in \mathbb{R}^{d+1} .

Suppose we construct the graph Laplacian by connecting each point to its nearest neighbors. We would now investigate the conditions under which the neighbors of each point belong to the

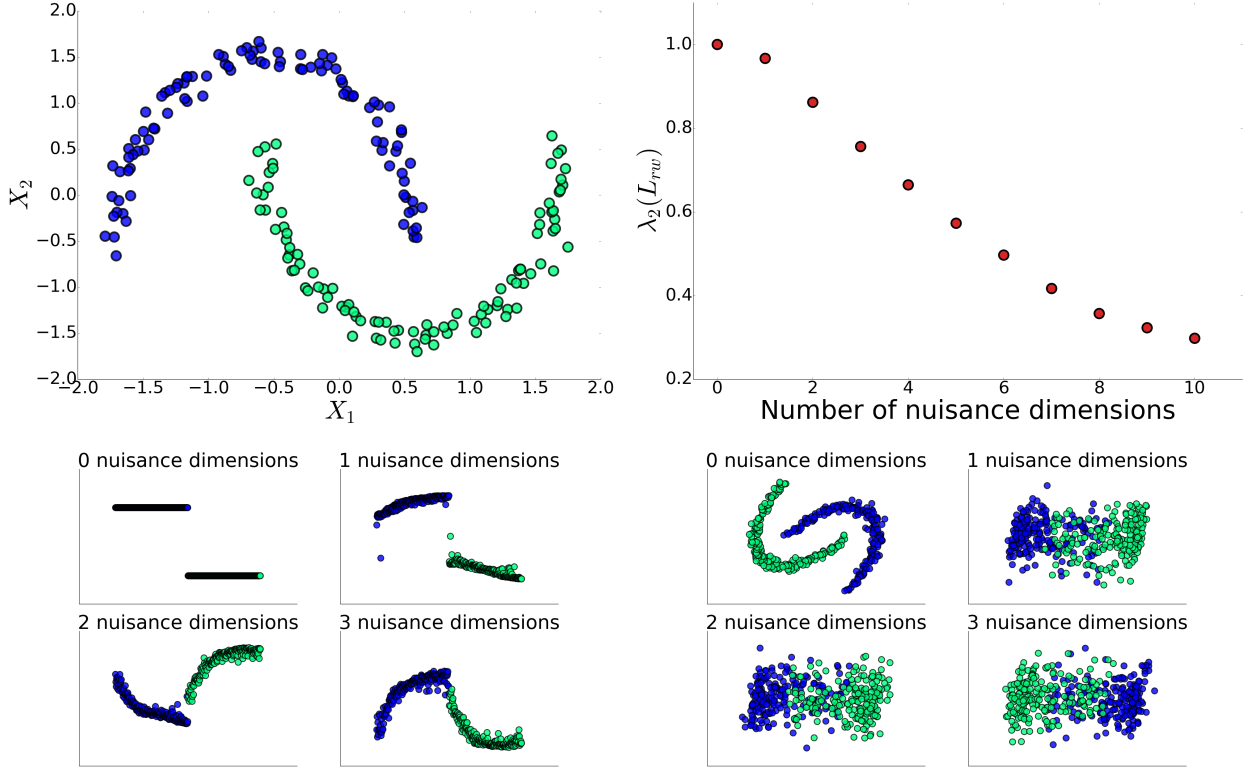


Figure 3: Two-moons experiment. Top Left: the original 2-dimensional dataset. Top right: the second largest eigenvalue of the random walk matrix \mathbf{L}_{rw} decreases as the number k of nuisance dimensions grows. This implies that the graph becomes more connected, and hence less clusterable, as the number of nuisance dimensions grows. Bottom left: the second largest eigenvector ψ_2 (y-axis) of \mathbf{L}_{rw} becomes less representative of the true cluster structure as k grows. The x-axis corresponds to the sample index. Bottom right: projecting the data onto the leading two principal directions (x and y axes) cannot recover the true cluster structure when $k > 0$.

correct cluster. Consider points x, y belonging to the same cluster. Then $(x - y) = (0, u_1, \dots, u_d)$ where $u_i \stackrel{\text{iid}}{\sim} N(0, 1)$, and therefore $\|x - y\|^2 \sim \chi_d^2$. Similarly, if x, y belong to different clusters, then $\|x - y\|^2 \sim r^2 + \chi_d^2$. We would now find conditions for n and d under which with high probability the neighbors of each point belong to the same cluster. In order to do that we utilize the Chi square measure-concentration bounds [40].

Lemma 3.1 ([40] P.1325). *Let $X \sim \chi_d^2$. Then*

1. $\mathbb{P}(X - d \geq 2\sqrt{d\gamma} + 2\gamma) \leq \exp(-\gamma)$
2. $\mathbb{P}(d - X \geq 2\sqrt{d\gamma}) \leq \exp(-\gamma)$

Given sufficiently small $\gamma > 0$ we can divide the segment $[d, d + r^2]$ to two disjoint segments of lengths $2\sqrt{d\gamma} + 2\gamma$ and $2\sqrt{d\gamma}$ (and solve for d in order to have the total length r^2). This yields

$$\sqrt{d} = \frac{r^2 - 2\gamma}{4\sqrt{\gamma}}. \quad (3)$$

The nearest neighbors of each point will be from the same cluster as long as all distances between points from the same cluster will be at most $d + 2\sqrt{d\gamma} + 2\gamma$ and all distances between points from different clusters will be at least $d + r^2 - 2\sqrt{d\gamma}$. According to lemma 3.1, this will happen

with probability at least $(1 - \exp(-\gamma))^{2n^2-n}$. Denoting this probability as $1 - \epsilon$ and solving for γ we obtain

$$\gamma \leq -\log(1 - \sqrt[2n^2-n]{1 - \epsilon}). \quad (4)$$

Plugging (4) into (3) we obtain

$$d = O\left(\frac{r^4}{-\log(1 - \sqrt[2n^2-1]{1 - \epsilon})}\right). \quad (5)$$

In particular, for fixed n and ϵ , equation (5) implies that the number of nuisance dimensions must be at most on the order of r^4 in order for the clusters to not mix with high probability. In addition, for a fixed r and ϵ , increasing the number of data points brings the argument inside the log term arbitrarily close to zero, which implies that for large data, the Laplacian is sensitive to the number of nuisance dimensions. We support these findings via experiments, as shown in Figure 4

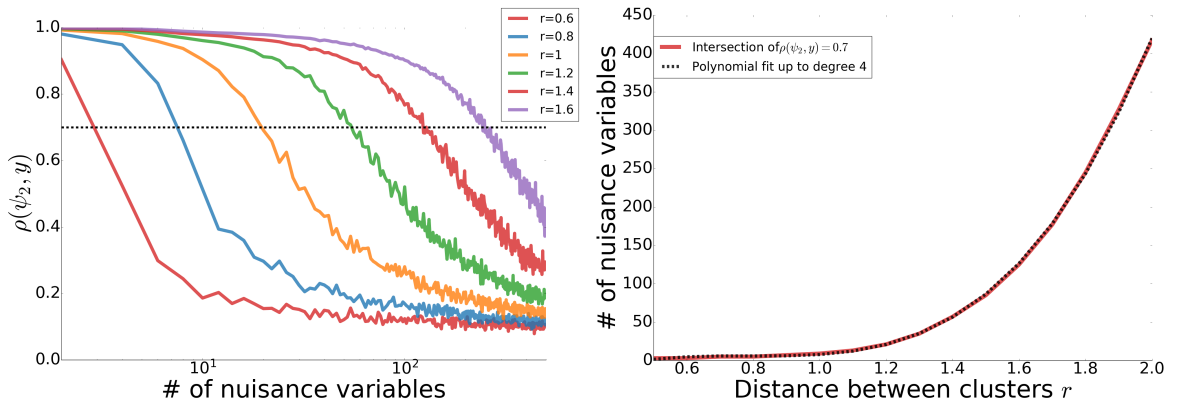


Figure 4: Two cluster datasets. We evaluate the influence of Gaussian nuisance variables on the Laplacian. We generate two clusters using 50 samples each with distance r apart in 1-D. We use d Gaussian nuisance variables and evaluate the leading non trivial eigenvector ψ_2 of the Laplacian. Left: correlation between the second eigenvector ψ_1 and the true cluster assignments y for different values of r . As the number of nuisance variables grows, the eigenvector becomes meaningless. As the distance between cluster grows more nuisance variables are required to “break” the cluster structure captured by ψ_2 . Right: by computing the intersection between the damped correlation curves and 0.7 (shown in the left plot) for different values of r we evaluate the relation between r and number of nuisance variables d required for breaking the cluster structure. This empirical result supports the analysis presented in 3.2 in which we show that $d = O\left(\frac{r^4}{-\log(1 - \sqrt[2n^2-1]{1 - \epsilon})}\right)$. For convenience we added a polynomial fit up to degree 4 presented as the black line.

4 Proposed Method

4.1 Rationale

Recall that the core component of the Laplacian score [27] is the quadratic term $\mathbf{f}^T \mathbf{L} \mathbf{f}$, which measures the inner product of the feature \mathbf{f} with the eigenvectors of the Laplacian \mathbf{L} . For

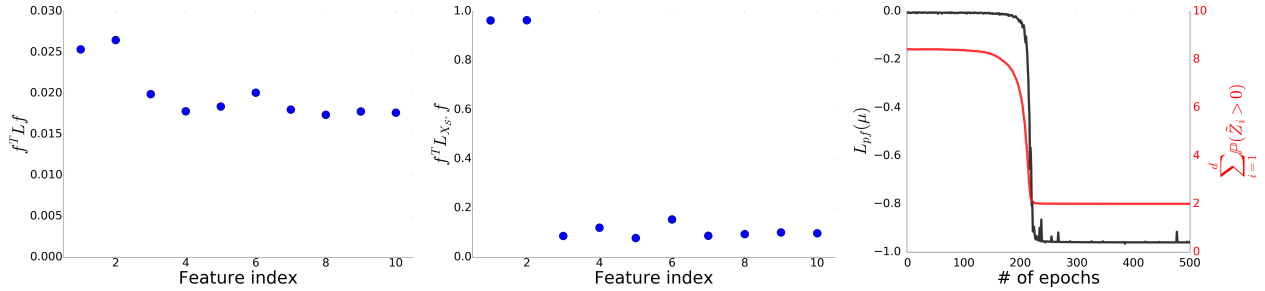


Figure 5: Demonstrating the information captured by the Laplacian Score based on the noisy-two moons dataset (illustrated in Fig. 3). The first two features are informative, while the rest of the variables are nuisance. Our goal is to train the differentiable stochastic gates for identifying the two informative features. Left: Laplacian score $\mathbf{f}^T \mathbf{L} \mathbf{f}$ at initialization, based on all 10 dimensions in total. The score for the informative features is slightly higher. Middle: Laplacian score, based on the gated Laplacian $\mathbf{f}^T \mathbf{L}_{X_{S^*}} \mathbf{f}$ at convergence of the gates. The informative features attain a substantial higher score based on the gated Laplacian. Right: the parameter-free loss (black line) and the average number of active gates (red line) as a function of the number of epochs.

$\mathbf{L} = \mathbf{L}_{rw} = \mathbf{D}^{-1} \mathbf{K}$ a large Laplacian score implies that \mathbf{f} has a large component in the subspace of eigenvectors corresponding to the largest eigenvalues of \mathbf{L} . Assuming that the structure of the data varies slowly, these leading eigenvectors (corresponding to large eigenvalues) manifest the main structures in the data, hence a large score implies that a feature contributes to the structure of the data. However, as we demonstrated in Section 3, in the presence of nuisance features, these leading eigenvectors become less representative of the true data structure. In this regime, one could benefit from evaluations of the Laplacian score when the Laplacian is computed based on different subsets \mathcal{S} of features, i.e., of the form $\mathbf{f}^T \mathbf{L}_{X_{\mathcal{S}}} \mathbf{f}$, where $\mathbf{L}_{X_{\mathcal{S}}}$ is the random walk Laplacian computed based on a subset of features $\{\mathbf{f}_{\ell}\}_{\ell \in \mathcal{S}}$. Such gated Laplacian score would produce a high score for the informative features \mathcal{S}^* when the Laplacian is computed only based on these features, that is when $\mathbf{L}_{X_{\mathcal{S}}} = \mathbf{L}_{X_{\mathcal{S}^*}}$. Searching over all different combinations of feature subsets is obviously infeasible even for a moderate number of features. Fortunately, we can use continuous stochastic “gating” functions to explore the space of feature subsets.

Specifically, we propose to apply differential stochastic gates to the input features, and compute the Laplacian score after multiplying the input features with the gates. Taking advantage of the fact that informative features are expected to have higher scores than nuisance ones, we penalize open gates. By applying gradient descent to a cost function based on $\mathbf{L}_{X_{\mathcal{S}}}$ we obtain the desired dynamic, in which gates corresponding to features that contain high level of noise will gradually close, while gates corresponding to features that are consistent with the true structures in the data will gradually get fully open. This is demonstrated in Fig. 5.

4.2 Differentiable Unsupervised Feature Selection (DUFS)

Let $\mathbf{X} \in \mathbb{R}^{m \times d}$ be a data minibatch. Let $\tilde{\mathbf{Z}} \in [0, 1]^d$ be the stochastic gates parametrized by $\boldsymbol{\mu} \in \mathbb{R}^d$, as defined in Section 2.3. For each mini-batch we draw a vector z of realizations from $\tilde{\mathbf{Z}}$ and define a matrix $\mathbf{Z} \in [0, 1]^{m \times d}$ consisting of m copies of z . We denote $\mathbf{X} \odot \mathbf{Z}$ as gated input, where \odot is an element-wise multiplication, also known as Hadamard product. Let $\mathbf{L}_{X \odot Z}$ be the random walk graph Laplacian computed on $\mathbf{X} \odot \mathbf{Z}$.

We propose two loss function variants. Both variants contain a feature scoring term

$$-\frac{1}{m}\text{Trace}[(\mathbf{X} \odot \mathbf{Z})^T \mathbf{L}_{\mathbf{X} \odot \mathbf{Z}}(\mathbf{X} \odot \mathbf{Z})],$$

and a feature selection regularization term $\sum_{i=1}^d \mathbb{P}(\tilde{\mathbf{Z}}_i \geq 0)$, following (2). In the first variant (6) the two terms are balanced using a hyperparameter $\lambda \geq 0$.

$$L(\mu; \lambda) := -\frac{1}{m}\text{Trace}[(\mathbf{X} \odot \mathbf{Z})^T \mathbf{L}_{\mathbf{X} \odot \mathbf{Z}}(\mathbf{X} \odot \mathbf{Z})] + \lambda \sum_{i=1}^d \mathbb{P}(\tilde{\mathbf{Z}}_i \geq 0). \quad (6)$$

Controlling λ allows for flexibility in the number of selected features. To obviate the need to tune λ , we propose a second loss function, which is parameter-free

$$L_{\text{param-free}}(\mu) := -\frac{\text{Trace}[(\mathbf{X} \odot \mathbf{Z})^T \mathbf{L}_{\mathbf{X} \odot \mathbf{Z}}(\mathbf{X} \odot \mathbf{Z})]}{m \sum_{i=1}^d \mathbb{P}(\tilde{\mathbf{Z}}_i \geq 0) + \delta}, \quad (7)$$

where δ is a small constant added to circumvent division by 0. The parameter-free variant (7) seeks to minimize the average score per selected feature, where the average is calculated as the total score (in the numerator) divided by a proxy for the number of selected features (the denominator). Minimizing both proposed objectives (6) and (7) will encourage the gates to remain open for features that yield high Laplacian score, and closed for the remaining features.

Our algorithm ¹ involves applying a standard optimization scheme (such as stochastic gradient descent) to objective (6) or (7). After training, we remove the stochasticity (ϵ_i in (1)) from the gates and retain features with parameters μ_i such that $\tilde{\mathbf{Z}}_i > 0$.

4.2.1 Raising L to the t 'th Power

Replacing the Laplacian \mathbf{L} in equations (6) and (7) by its t -th power \mathbf{L}^t with $t > 1$ corresponds to taking t random walk steps [39]. This suppresses the smallest eigenvalues of the Laplacian, while preserving its eigenvectors. We empirically found this to improve the performance of our proposed approach. We used $t = 2$ in our experiments.

5 Experiments

To demonstrate the relevance of the features selected by DUFS, our proposed approach, we begin by describing results obtained on the two moons dataset. We then report results obtained on several standard datasets, and compare them to current baselines. When applying the method to real data we perform feature selection based on Eq. (6) using several values of λ . Next, we perform clustering using k -means based on the leading 50, 100, 150, 200, 250, or 300 selected features and average the results over 20 runs. Leading features are identified by sorting the gates based on $\mathbb{P}(\tilde{\mathbf{Z}}_i)$ (see (2)). The number k of clusters is set as the number of classes and labels are utilized to evaluate clustering accuracy. The best average clustering accuracy is recorded along with the number $|\mathcal{S}|$ of selected features.

¹<https://github.com/Ofirlin/DUFS>

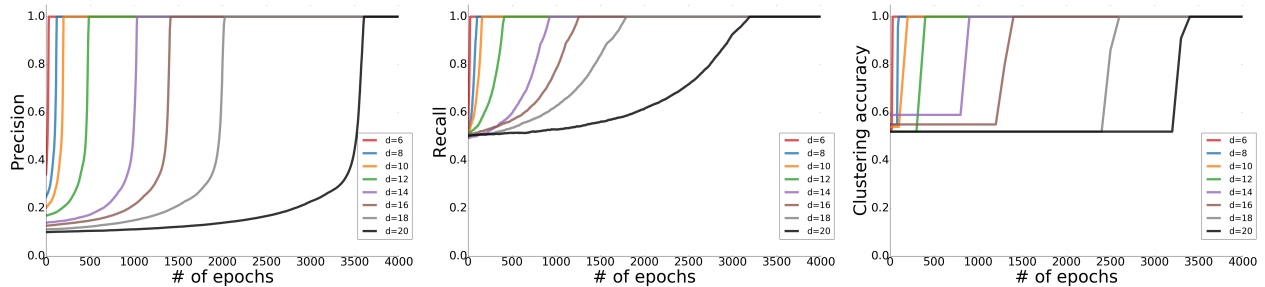


Figure 6: Evaluating the precision and recall of feature selection, as well as clustering quality as a function of epoch number. We apply the parameter-free loss variant (see (7)) of DUFFS on the noisy two-moons data with a total of d features. Left: precision of features selection. Here, precision is defined as the ratio between amount of retrieved informative features and all retrieved features, that is $\frac{\sum_{i=1}^2 P(\tilde{Z}_i > 0)}{\sum_{i=1}^d P(\tilde{Z}_i > 0)}$. Middle: recall of features selection. Here, recall is defined as the ratio between amount of retrieved informative features and all informative features, that is $\frac{\sum_{i=1}^2 P(\tilde{Z}_i > 0)}{2}$. Note that in all of these examples the gates converge to “deterministic” values. Namely $P(\tilde{Z}_i > 0) \simeq 1$ for informative features $i = 1, 2$ and $P(\tilde{Z}_i > 0) \simeq 0$ for the nuisance features $i = 3, \dots, d$. Right: clustering accuracy obtained with the retrieved features every 10 epochs. Here, clustering is performed using spectral clustering [25] with a Gaussian kernel.

5.1 Noisy Two Moons

In this experiment, we construct a dataset based on two moon-shaped classes, as shown in Fig. 3, concatenated with nuisance features. The first two coordinates $\mathbf{f}_1, \mathbf{f}_2$ are generated by adding a Gaussian noise with zero mean and variance of $\sigma_r^2 = 0.1$ onto two nested half circles, as presented in Fig. 3. Nuisance features $\mathbf{f}_i, i = 3, \dots, d$, are drawn from a multivariate Gaussian distribution with zero mean and identity covariance. The total number of samples is $n = 100$. Note that the small sample size makes the task of identifying nuisance variables more challenging.

We evaluate the convergence of the parameter-free loss function (7) using gradient decent. We use different number of features d and plot the precision and recall of feature selection throughout training (see Fig. 6). In all of the presented examples, perfect precision and recall are achieved at convergence.

5.2 Noisy Image Data

In the following experiment we evaluate our method on two noisy image datasets. The first is a noisy variant of MNIST [41], in which each background pixel is replaced by a random value drawn uniformly from $[0, 1]$ (see also [42]). Here we focus only on the digits ‘3’ and ‘8’. The second dataset is a noisy variant of PIXRAW10P (abbreviated PIX10), created by adding noise drawn uniformly from $[0, 0.3]$ to all pixels. In both datasets the images were scaled into $[0, 1]$ prior to the addition of noise. We applied to both datasets the DUFFS and LS approaches. In the top panels of Fig. 7 we present the leading 50 features retained on noisy MNIST along with the average clustering accuracy over 20 runs of k -means. In this case, DUFFS’ open gates concentrate at the left side of the handwriting area, which is the side that distinguishes ‘3’ from ‘8’. This allows DUFFS to achieve a higher clustering accuracy comparing to LS. We remark that the training was purely unsupervised and all label information was absent. The bottom panels of Fig. 7 show the leading 300 features retained on noisy PIX10 along with the average clustering accuracy. Here, DUFFS selects features which are more informative for clustering the face images. We refer the reader to Appendix S2 for additional information on the noisy image datasets along with extended results on noisy images.

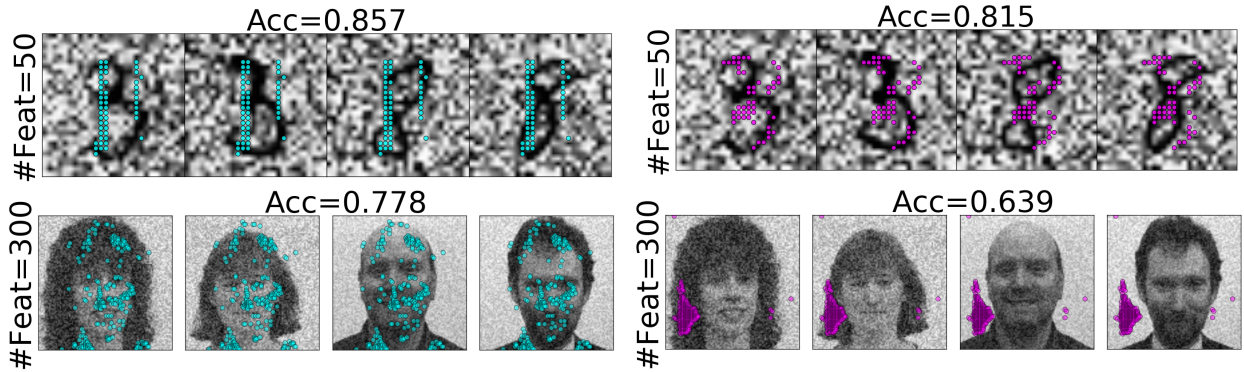


Figure 7: Noisy image experiments. Top: examples of noisy MNIST digits highlighted with the leading 50 features selected by DUFSS (left) and LS (right). Bottom: examples from the noisy PIX10 datasets overlaid with the leading 300 features selected by DUFSS (left) and LS (right). Here we present random samples from 4 out of 10 in total (see description in Table 1). This figure is best viewed in color. Note that the gray scale of MNIST images is inverted to improve visibility.

5.3 Clustering of Real World Data

In the following section, we evaluate the capabilities of the proposed approach (DUFSS) in clustering of real datasets. We use several benchmark datasets borrowed from [43]². The properties of all datasets are summarized in Table 1. In the first experiment we follow the analysis in [43]. We compare DUFSS to several baseline methods described in [43]. Specifically, we compare DUFSS to Laplacian Score [26] (LS), Multi-Cluster Feature Selection [44] (MCFS), Nonnegative Discriminative Feature Selection (NDFS) [45], Robust Unsupervised Feature Selection (RUFSS) [46] and Embedded Unsupervised Feature Selection (EUFSS) [43]. In table 2 we present the accuracy of clustering based on feature selected by DUFSS and all the five baselines³. As can be seen, in all but one case DUFSS selects features which lead to improved clustering results. Remarkably, on the PIX10 and ALLAML datasets, DUFSS’ superior clustering accuracy was obtained using a significantly smaller number of selected features. On the TOX-171 dataset, DUFSS outperforms MCFS, NDFS, RUFSS and performs comparably with EUFSS (while selecting less than half of the features selected by the latter).

Table 1: Description of the real world data used for empirical evaluation.

	PIX10	COIL20	Yale	ALLAML	TOX171	GLIOMA	PROSTATE
Features (D)	10000	1024	1024	7192	2000	5748	5966
Sample size	100	1444	165	72	62	171	102
Classes	10	20	15	2	2	4	2
Data type	Image	Image	Image	Biological	Biological	Biological	Biological

In the next experiment we evaluate the effectiveness of the proposed method for different numbers of selected features on 3 datasets. We compare DUFSS versus LS by performing k -means clustering using the features selected by each method. In Fig. 8 we present the clustering accuracies (averaged over 20 runs) based on the leading $\{50, 100, \dots, 300\}$ features. We see that DUFSS consistently selects features which provide higher clustering capabilities compared to LS.

²<http://featureselection.asu.edu/datasets.php>

³The results for Yale dataset are borrowed from [47]. For this dataset all methods are evaluated based on the leading $\{10, 20, \dots, 300\}$ features and the best accuracy is reported.

Table 2: Average clustering accuracy on several benchmark datasets borrowed from [43]. Accuracy is performed by applying k -means to the features selected by the different methods. The number of selected features is shown in parenthesis.

Datasets	LS	MCFS	NDFS	RUFS	EUFS	DUFS (Proposed)	All
PIX10	76.6 (150)	75.9 (200)	76.7 (200)	73.2 (300)	76.8 (150)	88.4 (50)	74.3
COIL20	55.2 (250)	59.7 (250)	60.1 (300)	62.7 (150)	63.4 (100)	65.8 (250)	53.6
TOX-171	47.5 (200)	42.5 (100)	46.1 (100)	47.8 (300)	49.5 (100)	49.1 (50)	41.5
ALLAML	73.2 (150)	68.4 (100)	69.4 (100)	72.2 (150)	73.6 (100)	74.5 (100)	67.3
PROSTATE	57.5 (300)	57.3 (300)	58.3 (100)	59.8 (50)	60.4 (100)	64.7 (150)	58.1
Yale	41.3	40.2	42.5	42.6	NA	45.7	38.3

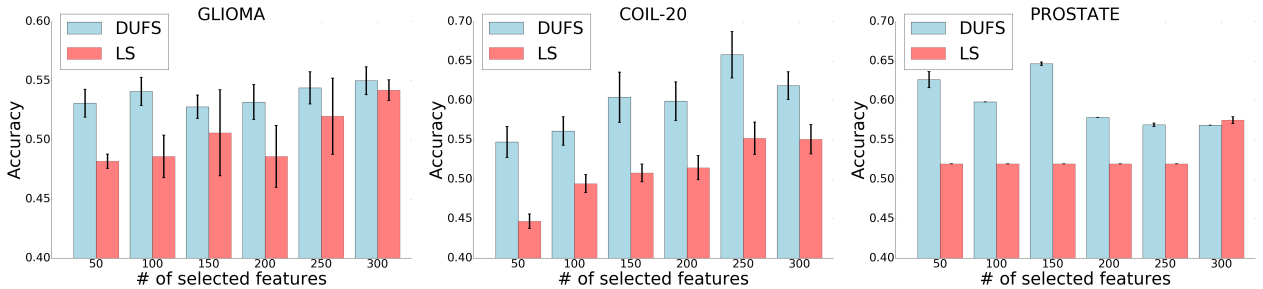


Figure 8: Clustering accuracy on three real world datasets. Clustering was performed on by applying k -means to features selected by DUFSS and LS. The averages and standard deviations based on 20 runs are shown.

6 Conclusions

In this paper, we propose DUFSS, a novel unsupervised feature selection method by introducing learnable Bernoulli gates into a Laplacian score. DUFSS has an advantage over the standard Laplacian score as it re-evaluates the Laplacian score based on the subset of selected features. We demonstrate that our proposed approach captures structures in the data that are not detected by mining the data with standard Laplacian, in the presence of nuisance features. Finally, we experimentally demonstrate that our method outperforms current unsupervised feature selection baselines on several real-world datasets.

Acknowledgements

The authors thank Stefan Steinerberger, Boaz Nadler and Ronen Basri for helpful discussions. This work was supported by the National Institutes of Health [R01GM131642, UM1DA051410, P50CA121974 and R61DA047037].

References

- [1] R. Battiti, “Using mutual information for selecting features in supervised neural net learning,” *IEEE Transactions on neural networks*, vol. 5, no. 4, pp. 537–550, 1994.

- [2] H. Peng, F. Long, and C. Ding, “Feature selection based on mutual information criteria of max-dependency, max-relevance, and min-redundancy,” *IEEE Transactions on pattern analysis and machine intelligence*, vol. 27, no. 8, pp. 1226–1238, 2005.
- [3] P. A. Estévez, M. Tesmer, C. A. Perez, and J. M. Zurada, “Normalized mutual information feature selection,” *IEEE Transactions on Neural Networks*, vol. 20, no. 2, pp. 189–201, 2009.
- [4] L. Song, A. Smola, A. Gretton, K. M. Borgwardt, and J. Bedo, “Supervised feature selection via dependence estimation,” in *Proceedings of the 24th international conference on Machine learning*. ACM, 2007, pp. 823–830.
- [5] L. Song, A. Smola, A. Gretton, J. Bedo, and K. Borgwardt, “Feature selection via dependence maximization,” *Journal of Machine Learning Research*, vol. 13, no. May, pp. 1393–1434, 2012.
- [6] J. Chen, M. Stern, M. J. Wainwright, and M. I. Jordan, “Kernel feature selection via conditional covariance minimization,” in *Advances in Neural Information Processing Systems*, 2017, pp. 6946–6955.
- [7] R. Kohavi and G. H. John, “Wrappers for feature subset selection,” *Artificial intelligence*, vol. 97, no. 1-2, pp. 273–324, 1997.
- [8] G. Stein, B. Chen, A. S. Wu, and K. A. Hua, “Decision tree classifier for network intrusion detection with ga-based feature selection,” in *Proceedings of the 43rd annual Southeast regional conference-Volume 2*. ACM, 2005, pp. 136–141.
- [9] Z. Zhu, Y.-S. Ong, and M. Dash, “Wrapper–filter feature selection algorithm using a memetic framework,” *IEEE Transactions on Systems, Man, and Cybernetics, Part B (Cybernetics)*, vol. 37, no. 1, pp. 70–76, 2007.
- [10] J. Reunanen, “Overfitting in making comparisons between variable selection methods,” *Journal of Machine Learning Research*, vol. 3, no. Mar, pp. 1371–1382, 2003.
- [11] G. I. Allen, “Automatic feature selection via weighted kernels and regularization,” *Journal of Computational and Graphical Statistics*, vol. 22, no. 2, pp. 284–299, 2013.
- [12] R. Tibshirani, “Regression shrinkage and selection via the lasso,” *Journal of the Royal Statistical Society. Series B (Methodological)*, pp. 267–288, 1996.
- [13] Y. Yamada, O. Lindenbaum, S. Negahban, and Y. Kluger, “Feature selection using stochastic gates,” *arXiv preprint arXiv:1810.04247*, 2018.
- [14] Y. Li, C.-Y. Chen, and W. W. Wasserman, “Deep feature selection: theory and application to identify enhancers and promoters,” *Journal of Computational Biology*, vol. 23, no. 5, pp. 322–336, 2016.
- [15] S. Scardapane, D. Comminiello, A. Hussain, and A. Uncini, “Group sparse regularization for deep neural networks,” *Neurocomput.*, vol. 241, no. C, pp. 81–89, Jun. 2017. [Online]. Available: <https://doi.org/10.1016/j.neucom.2017.02.029>
- [16] J. Feng and N. Simon, “Sparse-Input Neural Networks for High-dimensional Nonparametric Regression and Classification,” *ArXiv e-prints*, Nov. 2017.

- [17] S. Wang, Z. Ding, and Y. Fu, “Feature selection guided auto-encoder,” in *Thirty-First AAAI Conference on Artificial Intelligence*, 2017.
- [18] K. Han, Y. Wang, C. Zhang, C. Li, and C. Xu, “Autoencoder inspired unsupervised feature selection,” in *2018 IEEE International Conference on Acoustics, Speech and Signal Processing (ICASSP)*. IEEE, 2018, pp. 2941–2945.
- [19] A. Abid, M. F. Balin, and J. Zou, “Concrete autoencoders for differentiable feature selection and reconstruction,” *arXiv preprint arXiv:1901.09346*, 2019.
- [20] O. Alter, P. O. Brown, and D. Botstein, “Singular value decomposition for genome-wide expression data processing and modeling,” *Proceedings of the National Academy of Sciences*, vol. 97, no. 18, pp. 10 101–10 106, 2000.
- [21] R. Varshavsky, A. Gottlieb, M. Linial, and D. Horn, “Novel unsupervised feature filtering of biological data,” *Bioinformatics*, vol. 22, no. 14, pp. e507–e513, 2006.
- [22] D. Devakumari and K. Thangavel, “Unsupervised adaptive floating search feature selection based on contribution entropy,” in *2010 international conference on communication and computational intelligence (INCOCCI)*. IEEE, 2010, pp. 623–627.
- [23] M. Banerjee and N. R. Pal, “Feature selection with svd entropy: Some modification and extension,” *Information Sciences*, vol. 264, pp. 118–134, 2014.
- [24] V. M. Rao and V. Sastry, “Unsupervised feature ranking based on representation entropy,” in *2012 1st International Conference on Recent Advances in Information Technology (RAIT)*. IEEE, 2012, pp. 421–425.
- [25] A. Y. Ng, M. I. Jordan, and Y. Weiss, “On spectral clustering: Analysis and an algorithm,” in *Advances in neural information processing systems*, 2002, pp. 849–856.
- [26] M. Belkin and P. Niyogi, “Laplacian eigenmaps and spectral techniques for embedding and clustering,” in *Advances in neural information processing systems*, 2002, pp. 585–591.
- [27] X. He, D. Cai, and P. Niyogi, “Laplacian score for feature selection,” in *Advances in neural information processing systems*, 2006, pp. 507–514.
- [28] Z. Zhao and H. Liu, “Spectral feature selection for supervised and unsupervised learning,” in *Proceedings of the 24th international conference on Machine learning*, 2007, pp. 1151–1157.
- [29] P. Padungweang, C. Lursinsap, and K. Sunat, “Univariate filter technique for unsupervised feature selection using a new laplacian score based local nearest neighbors,” in *2009 Asia-Pacific Conference on Information Processing*, vol. 2. IEEE, 2009, pp. 196–200.
- [30] Z. A. Zhao and H. Liu, *Spectral Feature Selection for Data Mining (Open Access)*. CRC Press, 2011.
- [31] U. Von Luxburg, “A tutorial on spectral clustering,” *Statistics and computing*, vol. 17, no. 4, pp. 395–416, 2007.
- [32] X. He and P. Niyogi, “Locality preserving projections,” in *Advances in neural information processing systems*, 2004, pp. 153–160.

- [33] C. J. Maddison, A. Mnih, and Y. W. Teh, “The concrete distribution: A continuous relaxation of discrete random variables,” *arXiv preprint arXiv:1611.00712*, 2016.
- [34] E. Jang, S. Gu, and B. Poole, “Categorical reparameterization with gumbel-softmax,” 2017. [Online]. Available: <https://arxiv.org/abs/1611.01144>
- [35] C. Louizos, M. Welling, and D. P. Kingma, “Learning sparse neural networks through l_0 regularization,” *arXiv preprint arXiv:1712.01312*, 2017.
- [36] E. Jang, S. Gu, and B. Poole, “Categorical reparameterization with gumbel-softmax,” *arXiv preprint arXiv:1611.01144*, 2016.
- [37] A. Miller, N. Foti, A. D’Amour, and R. P. Adams, “Reducing reparameterization gradient variance,” in *Advances in Neural Information Processing Systems*, 2017, pp. 3708–3718.
- [38] M. Figurnov, S. Mohamed, and A. Mnih, “Implicit reparameterization gradients,” in *Advances in Neural Information Processing Systems*, 2018, pp. 441–452.
- [39] B. Nadler, S. Lafon, R. Coifman, and I. G. Kevrekidis, “Diffusion maps—a probabilistic interpretation for spectral embedding and clustering algorithms,” in *Principal manifolds for data visualization and dimension reduction*. Springer, 2008, pp. 238–260.
- [40] B. Laurent and P. Massart, “Adaptive estimation of a quadratic functional by model selection,” *Annals of Statistics*, pp. 1302–1338, 2000.
- [41] Y. LeCun, L. Bottou, Y. Bengio, and P. Haffner, “Gradient-based learning applied to document recognition,” *Proceedings of the IEEE*, vol. 86, no. 11, pp. 2278–2324, 1998.
- [42] Y. Qi, H. Wang, R. Liu, B. Wu, Y. Wang, and G. Pan, “Activity-dependent neuron model for noise resistance,” *Neurocomputing*, vol. 357, pp. 240–247, 2019.
- [43] S. Wang, J. Tang, and H. Liu, “Embedded unsupervised feature selection,” in *Twenty-ninth AAAI conference on artificial intelligence*, 2015.
- [44] D. Cai, C. Zhang, and X. He, “Unsupervised feature selection for multi-cluster data,” in *Proceedings of the 16th ACM SIGKDD international conference on Knowledge discovery and data mining*, 2010, pp. 333–342.
- [45] Z. Li, Y. Yang, J. Liu, X. Zhou, and H. Lu, “Unsupervised feature selection using nonnegative spectral analysis,” in *Twenty-Sixth AAAI Conference on Artificial Intelligence*, 2012.
- [46] M. Qian and C. Zhai, “Robust unsupervised feature selection,” in *Twenty-Third International Joint Conference on Artificial Intelligence*, 2013.
- [47] J. Li, L. Wu, H. Dani, and H. Liu, “Unsupervised personalized feature selection,” in *Thirty-Second AAAI Conference on Artificial Intelligence*, 2018.
- [48] A. Singer, R. Erban, I. G. Kevrekidis, and R. R. Coifman, “Detecting intrinsic slow variables in stochastic dynamical systems by anisotropic diffusion maps,” *Proceedings of the National Academy of Sciences*, vol. 106, no. 38, pp. 16 090–16 095, 2009.
- [49] Y. Keller, R. R. Coifman, S. Lafon, and S. W. Zucker, “Audio-visual group recognition using diffusion maps,” *IEEE Transactions on Signal Processing*, vol. 58, no. 1, pp. 403–413, 2009.

- [50] L. Zelnik-Manor and P. Perona, “Self-tuning spectral clustering,” in *Advances in neural information processing systems*, 2005, pp. 1601–1608.
- [51] O. Lindenbaum, M. Salhov, A. Yeredor, and A. Averbuch, “Kernel scaling for manifold learning and classification,” *arXiv preprint arXiv:1707.01093*, 2017.

Appendix

S1 Tuning the Kernel’s Bandwidth

It is important to properly tune the kernel scale/bandwidth σ_b , which determines the scale of connectivity of the kernel \mathbf{K} . Several studies have proposed schemes for tuning σ_b , see for example [48, 49, 50, 51]. Here, we focus on two schemes, a global bandwidth and a local bandwidth. The local bandwidth proposed in [50], involves setting a local-scale σ_i for each data point $\mathbf{x}_i, i = 1, \dots, n$. The scale is chosen using the L_1 distance from the k -th nearest neighbor of the point \mathbf{x}_i . Explicitly, the calculation for each point is

$$\sigma_i = \|\mathbf{x}_i - \mathbf{x}_k\|^2, i = 1, \dots, N, \quad (8)$$

where \mathbf{x}_k is the k -th nearest (Euclidean) neighbor of the point \mathbf{x}_i . We compute $\hat{\sigma}_b$ as the median over σ_i , then, the value of the kernel for points \mathbf{x}_i and \mathbf{x}_j is

$$K_{i,j} = \exp\left(-\frac{\|\mathbf{x}_i - \mathbf{x}_j\|^2}{\hat{\sigma}_b}\right), i, j \in \{1 \dots n\}. \quad (9)$$

This scale guarantees that at least half of the points are connected to k neighbors. For all experiments we use $k = 2$ as the number of nearest neighbors.

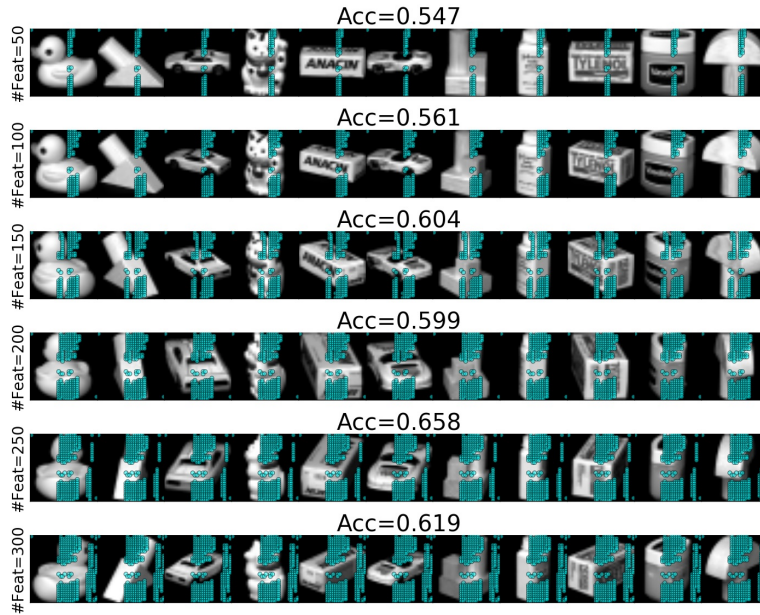
S2 Feature selection on Image Datasets

Here, we provide a deeper look into the features identified by the proposed method when applied to image data. We start with COIL20 which is a data that contains 20 objects captured at different viewing angles. In Fig. S1 we present the leading $\{50, 100, \dots, 300\}$ features selected by DUFFS and LS along with the average clustering accuracies based on the selected features. In this example DUFFS selects features which lie on the symmetry axis of COIL20, these features are more informative for clustering COIL20 since the values of rotated objects vary slowly on this axis. Next, we present a similar comparison on COIL100. COIL100 contains 7200 samples of 100 objects captured at different angles. Each image is of dimension $[128, 128, 3]$. In Fig. S2 we present the leading $\{50, 100, \dots, 300\}$ features selected by DUFFS and LS along with the average clustering accuracies based on the selected features. Here, feature selection is performed based on a black and white version of the RGB image and clustering is performed based on the corresponding subset of pixels from the RGB tensor.

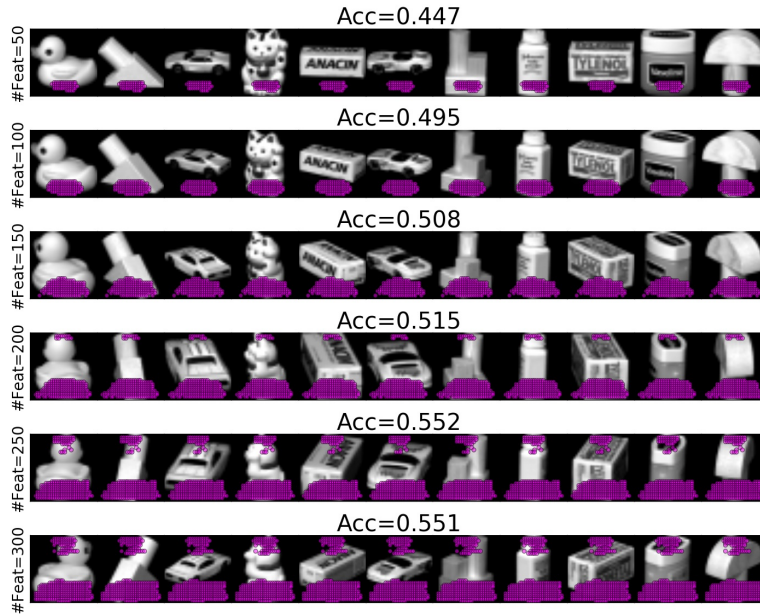
Finally, in Fig. S3 we present the results of application of DUFFS to the noisy MNIST dataset. This is an extension of the results presented in the paper. Specifically, we demonstrate the clustering accuracies based on the leading $\{50, 100, \dots, 300\}$ features selected by DUFFS and LS. In this experiment, we focused on a random subset of 1000 samples of the digits 3 and 8.

S3 Experimental Details

In this subsection we detail the parameters used throughout the experimental results. We use SGD for all the experiments which are conducted using Intel(R) Xeon(R) CPU E5-2620 v3 @2.4Ghz x2 (12 cores total). In all examples except COIL100 and COIL20 we use a full batch size for computing the kernel, for COIL100 and COIL20 the batch size is 1000. For all two-moons examples presented in Fig. 3 we use the parameter free loss term with a learning



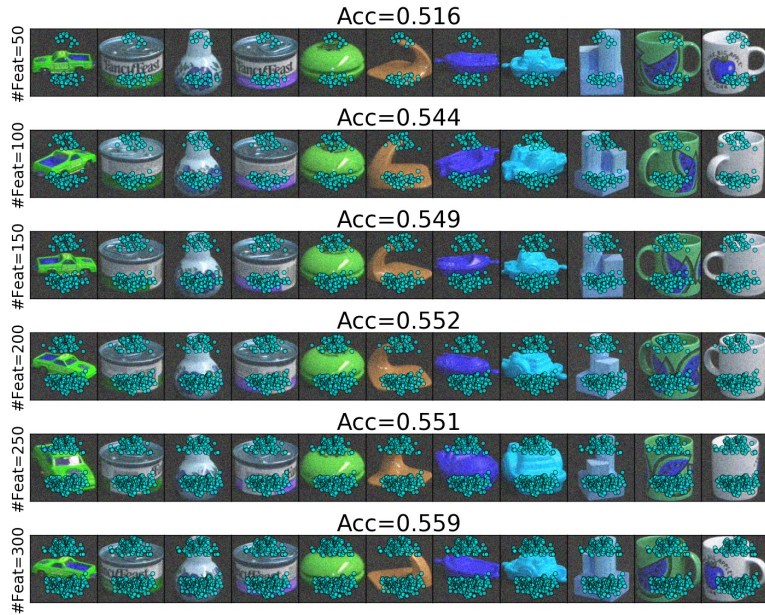
(a) DUFS



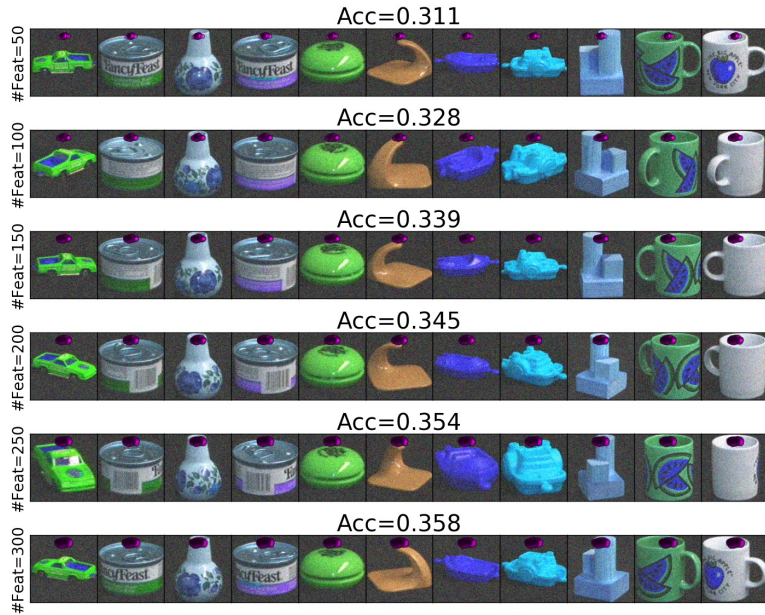
(b) LS

Figure S1: Features selected by DUFS and LS in the COIL20 dataset. Top: selected features (cyan dots) and clustering accuracy based on DUFS. Note that as COIL20 contains different angles of each object, the selected feature lie approximately on the symmetry axis. Bottom: selected features (magenta dots) and clustering accuracy based on LS.

rate (LR) of 1 and 5000 epochs. For PROSTATE data, we use a learning rate of 1, 12000 epochs and λ is evaluated in the range $[0.01, 1]$. For GLIOMA data we use a learning rate of 0.3, 12000 epochs and λ is evaluated in the range $[3, 30]$. For ALLAML data we use a learning rate of 0.3, 20000 epochs and λ is evaluated in the range $[1, 5]$. For COIL20 data we use a learning



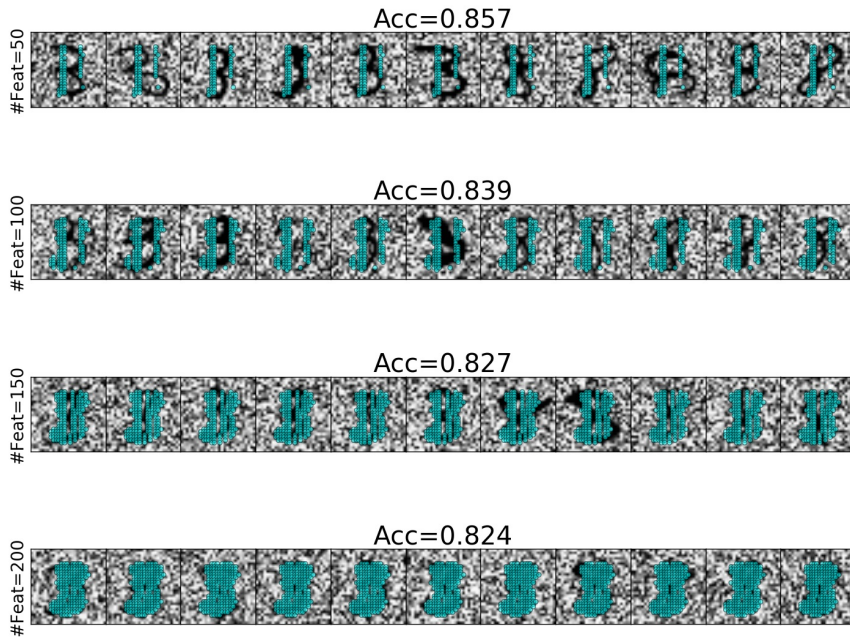
(a) DUFS



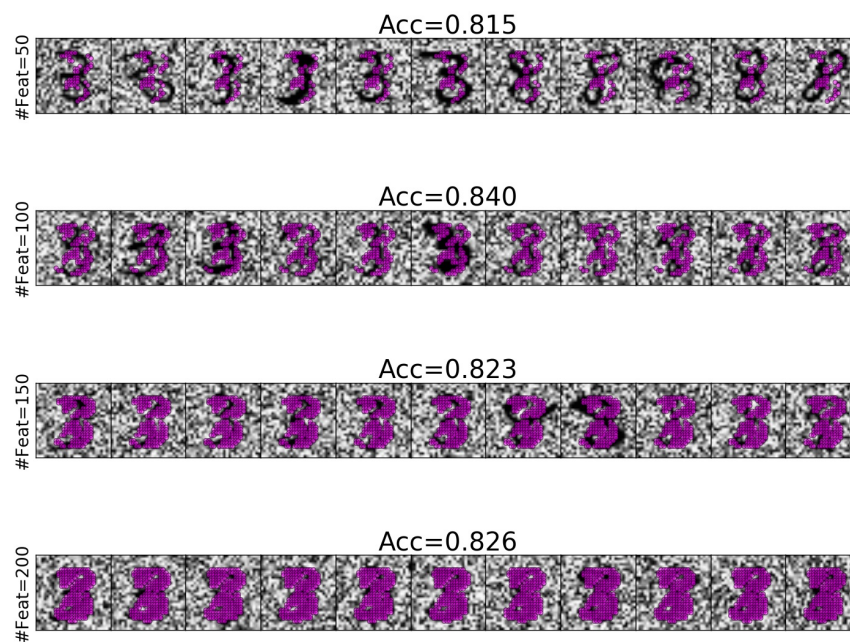
(b) LS

Figure S2: Same as for S1 but for the COIL100 dataset. Note that as COIL100 contains different angles of each object, the selected feature lie approximately on the symmetry axis. In this example, the LS also selects features on the symmetry axis, however the LS based selected features are condensed at a small region near the top part of the image. These features are informative for clustering wide vs. long objects but less informative for clustering all 100 objects.

rate of 0.3, 26000 epochs and λ is evaluated in the range $[0.01, 2]$. For COIL100 data we use a learning rate of 1, 6000 epochs and λ is evaluated in the range $[0.01, 2]$. For PIX10 data we use a learning rate of 0.3, 20000 epochs and λ is evaluated in the range $[0.05, 1]$.



(a) DUFS



(b) LS

Figure S3: Selected features on MNIST dataset. Top: selected features and clustering accuracy based on DUFS. Bottom: selected features and clustering accuracy based on LS. In this example, DUFS outperforms the LS when it is regularized to select a small number of features. However, when the regularization is set to select > 100 features in DUFS, the features with top scores in both methods are similar.